



Contents lists available at ScienceDirect

Chemical Physics Letters

journal homepage: [www.elsevier.com/locate/cplett](http://www.elsevier.com/locate/cplett)

Research paper

# Attosecond transient absorption spectroscopy of molecular nitrogen: Vibrational coherences in the $b' \ ^1\Sigma_u^+$ state

Erika R. Warrick<sup>a,b</sup>, Jens E. Bækhoj<sup>c</sup>, Wei Cao<sup>a,b</sup>, Ashley P. Fidler<sup>a,b</sup>, Frank Jensen<sup>d</sup>, Lars Bojer Madsen<sup>c</sup>, Stephen R. Leone<sup>a,b,e</sup>, Daniel M. Neumark<sup>a,b,\*</sup>

<sup>a</sup> Chemical Sciences Division, Lawrence Berkeley National Laboratory, Berkeley, CA 94720, USA

<sup>b</sup> Department of Chemistry, University of California, Berkeley, CA 94720, USA

<sup>c</sup> Department of Physics and Astronomy, Aarhus University, 8000 Aarhus C, Denmark

<sup>d</sup> Department of Chemistry, Aarhus University, 8000 Aarhus C, Denmark

<sup>e</sup> Department of Physics, University of California, Berkeley, CA 94720, USA

## ARTICLE INFO

## Article history:

Received 9 January 2017

In final form 7 February 2017

Available online xxxxx

## ABSTRACT

Nuclear and electronic dynamics in a wavepacket comprising bound Rydberg and valence electronic states of nitrogen from 12 to 15 eV are investigated using attosecond transient absorption. Vibrational quantum beats with a fundamental period of 50 femtoseconds persist for a picosecond in the  $b' \ ^1\Sigma_u^+$  valence state. Multi-state calculations show that these coherences result primarily from near infrared-induced coupling between the inner and outer regions of the  $b' \ ^1\Sigma_u^+$  state potential and the dark  $a'' \ ^1\Sigma_g^+$  state. The excellent spectral and temporal resolution of this technique allows measurement of the anharmonicity of the  $b' \ ^1\Sigma_u^+$  potential directly from the observed quantum beats.

© 2017 Elsevier B.V. All rights reserved.

## 1. Introduction

Tunable attosecond pulses of light in the extreme ultraviolet, which can be generated from table-top laser systems, provide a powerful tool for the investigation and control of ultrafast electronic and nuclear dynamics [1–3]. The large energy bandwidth of attosecond pulses makes them uniquely suited to the creation of coherent superpositions of multiple excited electronic states. In atoms, these consist of radial Rydberg state electronic wavepackets [4]. In molecules, excited electronic states can have widely varying potential shapes that support nuclear motion when triggered by excitation from the ground electronic state [5,6]. This is the case even for simple diatomic molecules such as nitrogen, as investigated here.

Attosecond transient absorption (ATA) spectroscopy is an all-optical technique that gives direct access to novel dynamics in highly excited states of atoms and molecules [7]. Due to the typically low intensity of attosecond pulses [8], the motion of the wavepacket that is launched by the attosecond pulse is monitored through the introduction of a strong near-infrared (NIR) few-femtosecond laser pulse that optically couples levels to neighboring states. In this type of experiment, the extreme ultraviolet

(XUV) absorption spectrum in the frequency range covered by the attosecond pulse is recorded as a function of the delay between the attosecond and femtosecond pulses. The attosecond pulse excites a wavepacket of dipole-allowed states, which creates a time dependent electronic charge distribution in the sample. Light emitted from this induced polarization interferes with the incident XUV field to give absorption features. When the NIR femtosecond pulse arrives, it modifies the induced polarization by ionization or coupling to neighboring states. This results in changes to the observed absorption spectrum due to electronic and vibrational coherences. ATA spectroscopy has exceptional time and energy resolution, limited only by the pulse durations, the stabilization of the time delay between the pulses used, and the resolution of the XUV spectrometer. Due to their resonant nature, quantum beats, including those with sub NIR laser cycle periods, can be observed with phase-locked pulses even if the NIR pulse is several femtoseconds in duration [9–11]. In atomic systems, ATA has been used to observe interference processes in electronic Rydberg wavepackets [10–13], to create transient light-induced states [9,14,15], to reconstruct correlated two electron dynamics [16], and to measure few femtosecond autoionization lifetimes [17–19].

Recent work has extended this technique to bound homonuclear diatomic molecular systems, showing that similar electronic processes can be measured [20–22]. The excited ion core Rydberg states above the first ionization potential of nitrogen are found to behave similarly to those of atomic species [20]. Lifetimes of

\* Corresponding author at: Department of Chemistry, University of California, Berkeley, CA 94720, USA

E-mail address: [dneumark@berkeley.edu](mailto:dneumark@berkeley.edu) (D.M. Neumark).

autoionizing Rydberg states of nitrogen were measured and quantum beats between electronic states observed and maximized through shaping of the initial wavepacket [21]. The increase in complexity of ATA experiments caused by the addition of nuclear degrees of freedom has stimulated the development of theoretical methods that can account simultaneously for electronic and nuclear vibrational motion in the interpretation of the dynamics [22–25]. Until now, experimental efforts have focused on molecular Rydberg states, where the excited electron is in a large, diffuse orbital that does not strongly perturb the molecular core or contribute to bonding [26].

In contrast, excitation to molecular valence states often involves the promotion of an electron from a bonding to an antibonding molecular orbital, resulting in a large geometry change with respect to the ground state, and a high degree of vibrational excitation in the excited state can occur as a consequence of the electronic excitation. Nitrogen has two states of valence character, the  $b' \ ^1\Pi_u$  and  $b' \ ^1\Sigma_u^+$  states, in the 12–15 eV energy range [27–30]. A schematic of the relevant potential energy curves is presented in Fig. 1. Single photon excitation to these states results in considerable nuclear motion, not considered before in the ATA studies of Rydberg state dynamics.

In this paper, we present a detailed experimental and theoretical treatment of ATA measurements on the bound Rydberg and valence states of nitrogen below the first ionization potential. An XUV pulse with a broad spectrum spanning 12–17 eV coherently excites the electronic states of nitrogen. A time-delayed, few femtosecond NIR pulse probes the evolution of the resulting electronic and vibrational wavepacket by optical coupling between the initially excited and neighboring vibronic states. We focus here on the extensive vibrational quantum beating in the  $b'$  state of nitrogen, which was noted, but not investigated, in our previous work [20]. The observed quantum beats are analyzed in detail to measure the anharmonicity of the potential and consider the effects of configuration mixing with neighboring Rydberg states of the same symmetry. A 12-electronic-state model based on the Born Oppenheimer approximation and involving coherent wavepacket motion in the vibrational degrees of freedom reproduces many of the spectral features of the experimental spectrum. A reduced model including only the  $b'$  valence state and the NIR-coupled  $a'' \ ^1\Sigma_g^+$  double-well state shows that distinct quantum beat features arise as the wavepacket traverses the inner and outer turning points of the  $b'$  state since these two regions are coupled to different wells of the  $a''$  state by the NIR probe pulse.

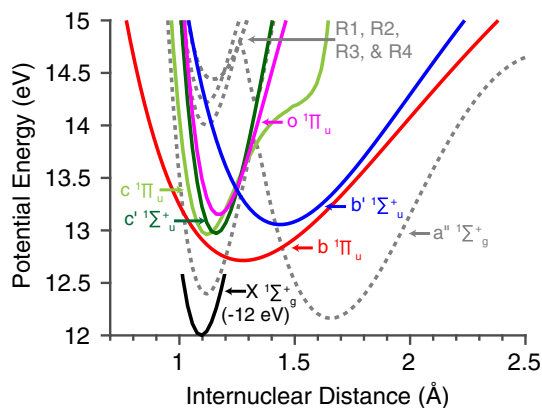


**Fig. 1.** A selection of nitrogen potential energy curves in the 12–15 eV energy range. The states shown in color (solid) can be accessed by the XUV pulse. Grey dashed states are dark states. The 12-curve model includes one additional state not shown here: the  $a' \ ^1\Pi_g$  valence state that spans energies from 8.55 to 11.3 eV. R1, R2, R3, and R4 are four Rydberg-like dark states. (For interpretation of the references to color in this figure legend, the reader is referred to the web version of this article.)

## 2. Experiment

The experimental setup is similar to that described previously [20]. Laser pulses from a commercial (Femtolasers) Ti:sapphire laser system with a multipass amplifier are spectrally broadened and temporally compressed using a gas-filled hollow-core fiber and chirped mirrors to generate 800  $\mu\text{J}$  of sub-6 fs NIR pulses at a 1 kHz repetition rate. The NIR pulses have a central wavelength of 1.6 eV (780 nm) with considerable bandwidth spanning 1.3–2.25 eV (950–550 nm). A beamsplitter divides the NIR beam into two arms. The majority (70%) of the beam passes through the optics necessary to implement double optical gating [31] to generate isolated attosecond pulses and is focused into a laser-drilled 1 mm pathlength cell in order to perform high harmonic generation using xenon gas. Using a 100 nm indium filter, the generating NIR field is blocked and the spectral output of the high harmonic generation process is limited to the 12–17 eV range. Temporal characterization was not performed, but the broad spectrum of the generated XUV radiation supports a sub-femtosecond Fourier-transform-limited pulse duration.

A gold-coated toroidal mirror focuses the XUV beam into a 1 mm long cell filled with nitrogen gas (backing pressure 11 torr). The remainder (30%) of the NIR pulse is recombined collinearly with the XUV beam before the target cell using an annular mirror. A variable time delay is introduced between the XUV and NIR pulses with the step size chosen to be either 0.3 or 1 fs to adjust measurement times based on the time-delay range to be studied. The NIR intensity at the target is approximately  $2 \times 10^{12} \text{ W/cm}^2$ . The spectrum of the XUV radiation after the target, which comprises both the transmitted XUV light and the dipole response of the sample, is measured using a flat field grating and an X-ray CCD camera. The spectrometer resolution is 14 meV at 14 eV. A 150 nm indium foil blocks the transmitted NIR light before the spectrometer.

## 3. Theory

In order to interpret the experimental results, numerical simulations of the combined nuclear and electronic motion are carried out using the  $N$ -curve model described in previous publications [23–25]. In this model, the total wave function of the molecule is expanded in  $N$  electronic Born-Oppenheimer (BO) states,  $\phi_j(z; R)$ :

$$\Psi(z, R, t) = \sum_{j=1}^N G_j(R, t) \phi_j(z; R), \quad (1)$$

where  $G_j(R, t)$  is the nuclear wave packet corresponding to the  $j$ th electronic state,  $R$  denotes the internuclear separation, and  $z$  represents all the electronic coordinates. To propagate the quantum mechanical state  $\Psi(z, R, t)$ , the expansion (1) is inserted into the time-dependent Schrödinger equation to obtain the following equations of motion

$$i \frac{d}{dt} G_i(R, t) = \sum_{j=1}^N \left[ H_i^{(0)} \delta_{ij} + V_{ij}(R, t) \right] G_j(R, t), \quad (2)$$

with  $H_i^{(0)} = -\frac{1}{2m_N} \frac{\partial^2}{\partial R^2} + E_{el,i}(R)$ ,  $m_N$  the reduced mass of the two nuclei,  $E_{el,i}(R)$  the BO potential energy curve (PEC),  $V_{ij}(R, t) = -F(t)d_{ij}^{el}(R)$ , where  $F(t)$  is the sum of the XUV and NIR fields, and  $d_{ij}^{el}(R)$  is the electronic dipole transition moment (EDTM) between the  $i$ th and the  $j$ th electronic states. The numerically obtained ATA spectra are calculated using  $N = 12$  electronic states. Guided by spectroscopic data [32], the  $N = 12$  states included in the model are chosen to reproduce the ATA spectrum of nitrogen in the energy range of the experiment as accurately as possible.

The adiabatic BO PECs were calculated by a Multi-Configurational Self-Consistent Field approach where all 10 valence electrons are correlated in 9 orbitals. The energies of the excited states are calculated by linear response methods, which also provide the EDTMs between the ground and excited states [33]. The EDTMs between excited states are calculated by quadratic response methods [34]. All calculations employ a doubly augmented cc-pVQZ basis set [35]. The calculations are carried out by the Dalton program package [36]. To obtain Eq. (2), all non-adiabatic couplings between electronic states are neglected. The adiabatic PECs obtained from the calculation described above must therefore be transformed into diabatic PECs for Eq. (2) to be accurate. For some diabatic PECs, this transform requires more than 25 adiabatic curves of the same symmetry. Fig. 1 shows a selection of PECs involved. The use of diabatic curves ensures that the EDTMs are smooth functions of the internuclear distance and that transitions between PESs only occur due to the dipole couplings.

For dilute gases, the modulation of the XUV pulse intensity profile is well estimated by [37]:

$$S(\omega, \tau) = \frac{4\pi n\omega}{c} \text{Im}[F_{\text{XUV}}^*(\omega, \tau)d(\omega, \tau)], \quad (3)$$

with  $\tau$  the time-delay,  $n$  the target density,  $c$  the speed of light,  $F_{\text{XUV}}(\omega, \tau)$  the Fourier transform of the XUV field, and  $d(\omega, \tau)$  the Fourier transform of the time-dependent dipole moment given as the quantum mechanical expectation value of the dipole operator, i.e. the expectation value of the total dipole operator in the state of Eq. (1).  $d(\omega, \tau)$  therefore acts as the link between the microscopic single-system calculations and the macroscopic field propagation.  $S(\omega, \tau)$  as calculated numerically relates to the optical density (OD) reported in the experimental ATA spectra as

$$\text{OD}(\omega) = -\log \left[ 1 + \frac{S(\omega, \tau)}{|F_{\text{XUV}}(\omega, \tau)|^2} \right] \cong -\frac{S(\omega, \tau)}{|F_{\text{XUV}}(\omega, \tau)|^2}, \quad (4)$$

with the approximation above being accurate for dilute gas targets.

The calculations assume a single molecular orientation rather than a spherically symmetric distribution of orientations, which is expected to be a better model for the unaligned target [25]. The single orientation used is chosen such that EDTMs with non-zero components parallel to the molecular axis and EDTMs with non-zero components in either of the two orthogonal directions have equal weights in the calculation. The single-orientation calculations were tested against calculations where contributions from all orientations are coherently summed for selected time-delays with very good agreement [25]. Both propagation through a macroscopic medium [37] and integration over the angular distribution are formidable numerical tasks, so the fact that ATA spectra can be calculated without considering these allows us to treat surprisingly complex systems.

The calculations assume an 8.9 fs 760 nm NIR pulse (FWHM of intensity profile) with a peak intensity of  $2.2 \times 10^{12}$  W/cm<sup>2</sup> and a 300 as 78 nm XUV pulse with a peak intensity of  $5 \times 10^7$  W/cm<sup>2</sup>. To reproduce the width of the absorption lines observed in experiments, the calculated time-dependent dipole moment is damped using a window function. The timescale on which the window function damps the dipole moment must be chosen such that the lowest frequency components of interest, i.e. the energy differences between neighboring vibrational states, are resolved. In the  $b$  and  $b'$  curves, these energy differences are approximately 0.08 eV, corresponding to a vibrational period of 52 fs, so the results presented in Fig. 2(b) are calculated using a 120 fs window function [23]. Later, we will be interested in the modulations in specific absorption lines as a function of time delay for hundreds of femtoseconds. In this case, a 1.20 ps window function is used, resulting in narrower absorption lines than are found in the

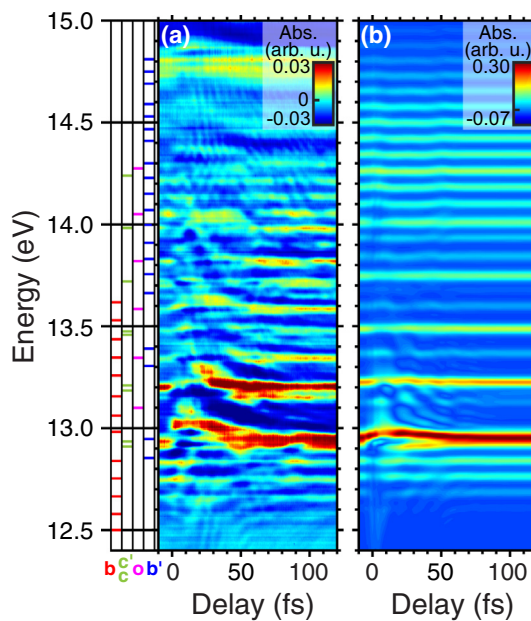


**Fig. 2.** (a) Delay-dependent absorption of nitrogen for time delays less than 120 fs in the 12.4–15 eV energy range. The color scale represents absorption. Delay steps of 0.3 fs were accumulated. Positive delays mean that the NIR pulse precedes the XUV pulse. The energetic locations of the vibrational levels of the  $b$   $^1\Pi_u$  (red),  $c$   $np\pi$   $^1\Pi_u/c'$   $np\sigma$   $^1\Sigma_u^+$  (green),  $o$   $3s\sigma$   $^1\Pi_u$  (pink) and  $b'$   $^1\Sigma_u^+$  (blue) states are shown to the left of the spectrum [27–30]. (b)  $-S(\omega, \tau)$  of Eq. (3) calculated using the ( $N=12$ ) curve model of Section 3. The theoretical results are obtained using a window function [23] to damp the polarization of the target gas within 120 fs. (For interpretation of the references to color in this figure legend, the reader is referred to the web version of this article.)

experiment, but still allowing for an investigation of the time-delay dependent modulations of the lines.

#### 4. Results

Transient absorption spectra of nitrogen from 12.4 to 15 eV as a function of the XUV-NIR time delay are shown in Figs. 2(a) and 3(a). Positive time delays signify that the NIR pulse arrives after the XUV pulse. The color scale represents Fourier filtered absorbance, defined as the negative logarithm of the transmitted XUV light divided by a reference spectrum constructed from the transmitted spectrum using a low pass Fourier filter. The filter excludes the high frequency spectral modulations that come from absorption features while capturing the slow modulation of the incident XUV spectrum [16]. This self-referencing of the absorbance measurements for each time delay eliminates noise caused by transient shifts of the XUV spectrum over time.

The XUV pulse excites numerous overlapping vibrational series associated with states of Rydberg and valence character [27–30]. The positions of vibrational levels associated with each electronic transition are marked to the left of Figs. 2(a) and 3(a). To briefly summarize, there are two Rydberg series converging to the ground state,  $X^2\Sigma_g^+$ , of the molecular ion. They are  $np$  states of different symmetries,  $3p\pi$   $^1\Pi_u$  and  $3p\sigma$   $^1\Sigma_u^+$ , denoted as  $c$  and  $c'$ . Contributions from the  $4p$  members of the series, known as  $e/e'$ , occur above 14.39 eV. The  $o$  series is an additional Rydberg series built on the  $A^2\Pi_u$  excited molecular ion core,  $3s\sigma$   $^1\Pi_u$ . Two valence states,  $b$   $^1\Pi_u$  and  $b'$   $^1\Sigma_u^+$ , are also present in this spectral region, and can be recognized by their closely spaced vibrational levels.

Fig. 2(a) shows the time-delay-dependent absorption for the first 120 fs after XUV excitation, accumulated using delay steps of 300 attoseconds. A dominant behavior for all the states in this region is energy-level shifting. This effect is seen clearly in the first

$c/c'$  Rydberg levels around 13 eV, where the spectral features are strongly distorted energetically towards higher energies for the first 50 fs. At higher energies, around 14.0 eV, pronounced oscillations in numerous absorption features are observed with a period of approximately 7 fs in addition to the shifting. These are due to Rydberg state electronic coherences in the  $e/e'$  state, similar to those previously reported for Rydberg states of nitrogen above 15 eV [20]. Fig. 2(b) depicts the numerically obtained spectrum calculated using the  $N = 12$  curve model described in Section 3 with a window function damping the polarization within 120 fs. This spectrum captures the line shape changes well for the lowest photon energies. For photon energies above 13.5 eV, the agreement between Fig. 2(a) and (b) is not quite as good. The breakdown of the model occurs because of electronic states not included in the expansion of Eq. (1), such as the  $e/e'$  and higher energy Rydberg states, which affect the optical properties of nitrogen at these higher energies.

Fig. 3(a) shows an extended experimental time delay range out to 1 ps obtained using 1 fs steps. The same short-time behavior appears in this spectrum, but longer period oscillations, approximately 50 fs, are present in individual vibrational levels of the  $b$  and  $b'$  valence states. A Fourier transformation performed along the time delay axis of the absorption spectrum can decompose the oscillation frequencies in each absorption level, shown in Fig. 3(b) and, over a narrower energy range, in Fig. 4. The Fourier analysis reveals numerous near-vertical sequences of frequencies that are evenly spaced in the frequency domain by about 0.08 eV. They form two distinct groups in energy, with one group at energies below 13.25 eV, where absorption features due to the valence  $b$  state dominate the static absorption spectrum, and the other group spanning energies from 13.5 eV to about 15 eV, where the strongest absorption features are due to the valence  $b'$  state. The  $b$  state oscillations were discussed over a smaller delay window in a previous paper [20] and will not be explored further here.

Fig. 4 shows the spectral region where the valence  $b'$  state is observed, shown in a limited Fourier frequency region below 0.3 eV. The energies of the vibrational levels of the  $b'$  valence and  $X^2\Sigma_g^+$  ion core Rydberg states with  $n = 3$  ( $c/c'$ ) and  $n = 4$  ( $e/e'$ ) in this region are marked with horizontal lines. Each  $b'$  state vibrational level shows a similar pattern of oscillation frequencies at multiples

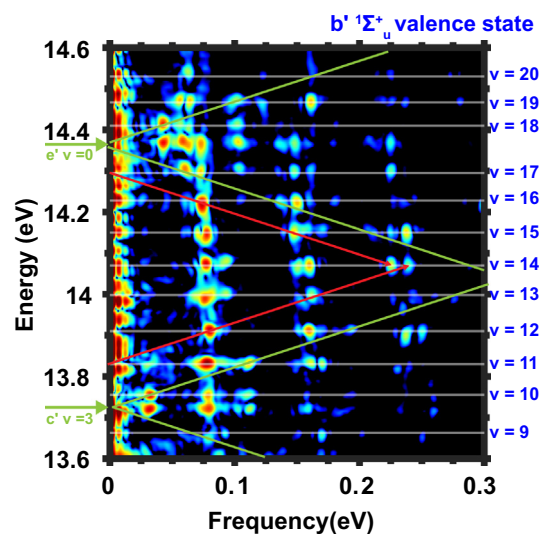


Fig. 4. Fourier analysis of the delay dependent transient absorption of nitrogen from Fig. 3(b) presented in the limited 13.6–14.6 eV energy range. The positions of the vibrational levels of the  $b'$  state are marked with grey horizontal lines [28,30]. Red lines of slope  $\pm 1$  have been added to illustrate NIR-induced coupling processes. Perturbing Rydberg states built on the ground state,  $X^2\Sigma_g^+$ , of the molecular ion with  $n = 3$  ( $c/c'$ ) and  $n = 4$  ( $e/e'$ ) have been marked with green arrows and lines of slope  $\pm 1$  [28,29]. (For interpretation of the references to color in this figure legend, the reader is referred to the web version of this article.)

of the 0.08 eV vibrational period of this state. Many of these frequencies appear as closely spaced doublet features along the horizontal lines due to anharmonicity. Additional quantum beats are seen corresponding to particular Rydberg state vibronic levels, indicated by the green arrows in Fig. 4. These attributes of Fig. 4 are discussed in detail below.

## 5. Discussion

The time dependent oscillations in the nitrogen ATA spectrum are quantum beats that give information about the potential

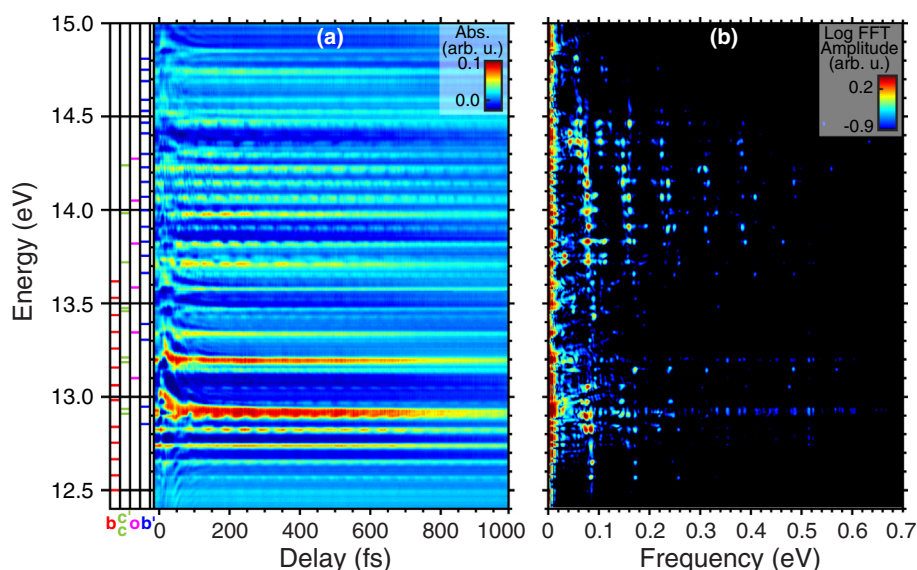
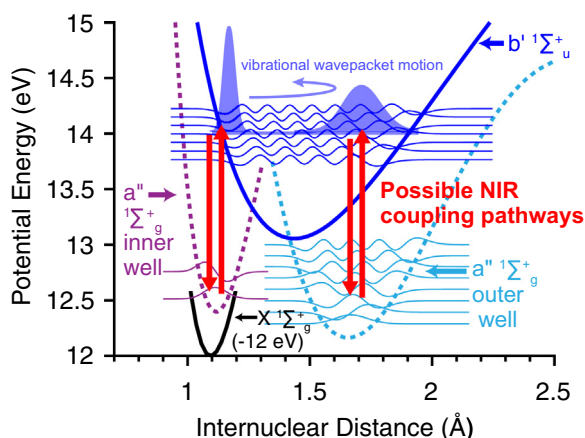


Fig. 3. (a) The delay dependent absorption of nitrogen for time delays out to 1 ps shown in the 12.4–15 eV energy range. The color scale represents absorption. Delay steps of 1 fs were used. Positive delays mean the attosecond XUV pulse precedes the NIR pulse. The energetic locations of the vibrational levels of the  $b^1\Pi_u$  (red),  $c\ n\pi^1\Pi_u/c'\ n\pi\sigma^1\Sigma_u^+$  (green),  $o\ 3s\sigma^1\Pi_u$  (pink) and  $b^1\Sigma_u^+$  (blue) states are shown to the left of the spectrum [27–30]. (b) Fourier analysis of the spectrogram in (a) with respect to the delay axis plotted on a log color scale. (For interpretation of the references to color in this figure legend, the reader is referred to the web version of this article.)



**Fig. 5.** Schematic of possible pathways by which the NIR pulse can couple adjacent vibrational levels in the  $b'$  state through the  $a'' \ ^1\Sigma_g^+$  inner or outer potential well. The wavepacket vibrational levels  $v = 10$ – $16$  are illustrated.

energy curves of the system, the nuclear dynamics in these curves, and how bright and dark states couple in the NIR field. In ATA experiments, quantum beats are caused by 2-photon NIR-induced coupling between two bright state levels through a resonant dark state [9,11–13,16,20,22].

The exact NIR-induced coupling mechanism that allows for the observation of the quantum beating in the  $b'$  valence state cannot be determined from the experimental observations alone. In the energy range accessible by the NIR pulse, dark states of both Rydberg and valence character have been found [38]. Of particular interest is an avoided crossing between the  $a'' \ ^1\Sigma_g^+$  Rydberg and  $^1\Sigma_g^+(II)$  valence state, confirmed experimentally by considerable energetic perturbations of the observed vibrational levels of these two states [39,40]. The resulting double well potential of the mixed  $a'' \ ^1\Sigma_g^+$  Rydberg and  $^1\Sigma_g^+(II)$  valence states is the only known bound

dark state that is energetically resonant with the  $b'$  valence state via 1 NIR photon. A schematic of the proposed coupling mechanisms allowing for the observation of  $b'$  valence state quantum beating is shown in Fig. 5.

### 5.1. Mechanism of NIR coupling

$N$ -curve model simulations were performed in order to confirm the proposed coupling scheme and determine the effects of internuclear distance-dependent coupling to the two wells of the mixed  $a'' \ ^1\Sigma_g^+$  Rydberg/valence dark state. The full 12-curve model producing the spectrum in Fig. 2(b) was propagated for 400 fs in order to capture the long period oscillations. The predicted ATA results versus time delay and vibrational state are shown as the black lines in Fig. 6(a) for the  $v = 8$ – $19$  vibrational levels in the  $b'$  state. The red lines show the results from a simplified model that includes only the ground state, the  $b'$  bright valence state, and the  $a''$  dark state. The two calculations give very similar results, providing compelling evidence that the delay-dependent structures of the  $b'$  absorption lines are a result of NIR-field induced couplings to the  $a''$  curve. No other dark states in the 12-curve model are strongly coupled to the  $b'$  state.

While each of the simulated  $b'$  vibrational levels shows similar frequency components in the Fourier transform, they are revealed to have very different structure when their time dependent absorption dynamics are plotted as in Fig. 6. Many of the levels above  $v = 14$  have a dominant broad, flat-top structure that appears with a 50 fs period, consistent with the classical oscillation period of the  $b'$  state predicted by the vibrational spacing. However, some of the levels also have narrow peaked contributions that also occur every 50 fs. In levels where both types of features occur, they appear to be out of phase, with the narrow contributions occurring when the broad ones are minimized. The two out-of-phase contributions can also be seen in the experimental absorption spectrogram, as shown in Fig. 7 for the  $b' \ v = 15$  level

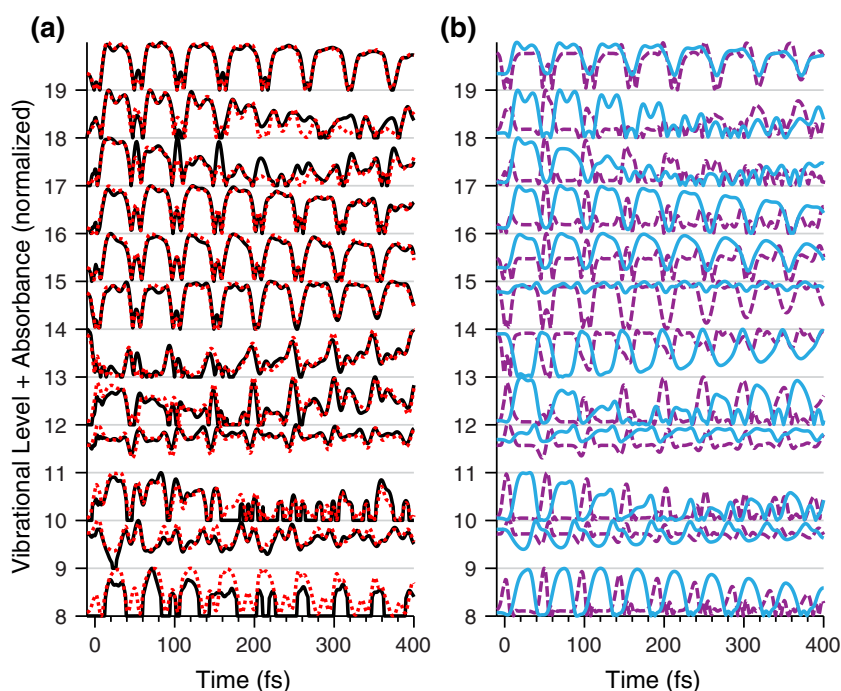


**Fig. 6.** Calculated absorption lineouts for selected  $b'$  vibrational levels,  $v = 8$ – $19$ . Each lineout has been normalized to its maximum absorbance and shifted vertically by its vibrational number in the  $b'$  state. (a) The black (solid) lineouts are from the full 12-curve model while red (dotted) lineouts are from a simplified 3-curve model including the ground,  $b'$ , and  $a''$  states. (b) The purple (dashed) and cyan (solid) lineouts are from 3-curve models where only the inner or outer wells of the  $a''$  state have been included respectively.

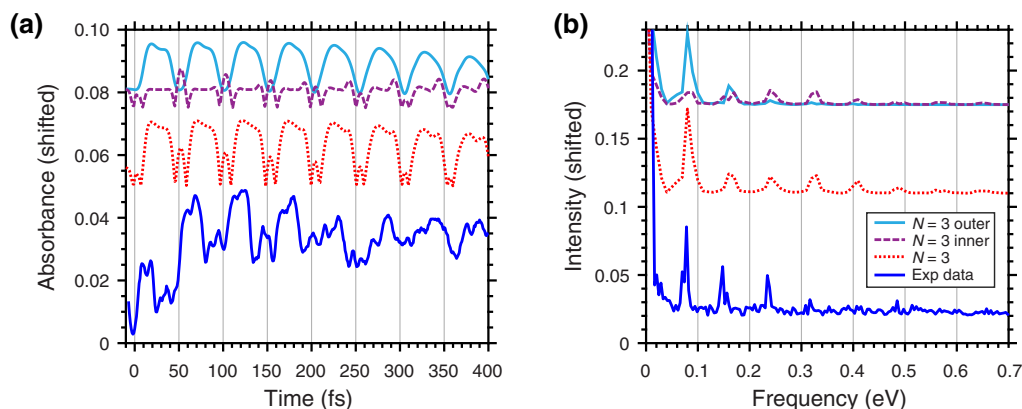


**Fig. 7.** (a) Absorption lineouts for the 14.18 eV  $b' v = 15$  vibrational level. The blue (black) line is the experimental data. The other colors denote different  $N$ -curve models. Red (dotted) is a simplified 3-curve model including the ground,  $b'$ , and  $a''$  states. The purple (dashed) and cyan (grey) lineouts are from 3-curve models where only the inner or outer wells of the  $a''$  state have been included, respectively. The lines have been shifted and scaled for clarity. (b) The respective Fourier transforms of the lineouts. (For interpretation of the references to color in this figure legend, the reader is referred to the web version of this article.)

(blue line). To match the delay range calculated by theory, only the first 400 fs of the experimental data are shown, but quantum beating in this level persists for more than a picosecond.

Overall, the observed behavior is due to the internuclear distance-dependent contributions of the coupling to the  $a''$  dark state. The  $N = 3$  curve model was modified to include either the inner (Rydberg-like) or outer (valence-like) part of the  $a''$  state only. The resulting absorption lineouts are shown in Fig. 6(b), with the purple corresponding to the inner well and the cyan lineouts corresponding to the outer well. In general, the outer well is responsible for the broad temporal features while the inner well creates the narrow temporal structures. The sum of these two contributions reproduces the  $N = 3$  model, as shown in the full  $a''$  state computation shown in Fig. 6(a).

These effects are considered in more detail in Fig. 7(a) and (b), which show the simulated and experimental absorption lineouts for the  $b' v = 15$  level and the corresponding Fourier transforms. Contributions from the inner and outer wells are shown as the purple and cyan lines, respectively, in both panels. The outer well of the  $a''$  state mainly couples neighboring vibrational levels in the  $b'$  well, resulting in strong  $\Delta v = \pm 1$  and weaker  $\Delta v = \pm 2$  quantum beat frequencies in the absorption spectrum, and creating the broad structure in the time domain. The inner well can couple states from  $\Delta v = \pm 1$  to  $\pm 4$  with similar strength, resulting in the narrow, peaked structure in the time domain.

The difference in which  $b'$  vibrational levels couple through the dark state wells can be explained by the difference in Franck-Condon overlap between each well and the  $b'$  bright state, illustrated schematically in Fig. 5. The inner turning point of the  $b'$  well lies at a similar bond length as the minimum of the  $a''$  state inner well. This results in similarly sized Franck-Condon factors for small and large  $\Delta v$  transitions in the  $b'$  state through the  $a''$  inner well. In contrast, the outer arms of the blue and cyan potentials are nearly parallel, so the Franck-Condon factors will vary much more with vibrational level and lead to fewer quantum beat frequencies. These internuclear distance-dependent differences in coupling between the wells provide an intuitive mechanism for visualizing the movement of the  $b'$  state wavepacket through the observed out-of-phase broad and narrow contributions to the quantum beat structure.

## 5.2. Direct measurement of vibrational anharmonicity

The high frequency resolution of the ATA technique provides a direct measure of the anharmonicity of the  $b'$  potential energy

curve. Different frequencies can be observed from processes that optically couple different vibrational levels of the  $b'$  state through either the gain or loss of the same number of vibrational quanta. This causes two closely spaced peaks in Fourier frequency. A specific example is the quantum beats due to the  $\Delta v = \pm 3$  transitions to the same  $b' v = 14$  vibrational level at 14.07 eV, illustrated by the red lines in Fig. 4. Oscillations caused by population transfer from the higher  $b' v = 17$  level at 14.30 eV to the  $b' v = 14$  level occur at a frequency 10 meV lower than those caused by coupling from the  $b' v = 11$  level at 13.83 eV due to the anharmonicity of the PEC.

Vibrational anharmonicity is not the only process responsible for extra peaks in the Fourier spectrum in Fig. 4. Two states of Rydberg character contribute to several low frequency oscillations as well. The  $v = 3$  level of the  $c'$  state at 13.72 eV is strongly coupled by the NIR pulse to its neighboring  $b'$  state, the  $v = 10$  level at 13.76 eV, leading to  $\sim 100$  fs oscillations in both states, and also causing oscillations that are slightly higher in frequency than the overtone contributions in the  $b' v = 11, 12$  and 13 levels. The  $v = 0$  level of the  $e'$  state at 14.39 eV shows significant long period oscillations as well. It strongly perturbs the vibrational spacing in the  $b'$  state, resulting in the additional structure in the  $b' v = 16$ –19 region of the valence state vibrational levels. This Rydberg-valence interaction is a result of homogeneous configuration mixing, which has been studied in these states in nitrogen both theoretically and experimentally through rotational level analysis of static absorption measurements [27,41,42]. It occurs between Rydberg and valence states of the same symmetry when the energy levels of the two different curves are close in energy and results in states that are of mixed electronic character [41]. A nonadiabatic theoretical analysis found that the  $v = 0$  level of the  $e'$  state is mostly valence  $b'$  state like in character [42]. Due to this state mixing, these Rydberg state levels behave similarly to the valence state levels in the time-resolved experiment.

To directly extract the anharmonicity of the  $b'$  potential well from the time dependent absorption spectrum, a simple peak picking analysis was performed to isolate the frequency components of the  $\Delta v = +1, 2$  and 3 transitions in each vibrational spectral line. These are plotted in Fig. 8. The pronounced deviations of the resulting series emphasize the strong perturbations of the  $b'$  vibrational level spacing discussed above, which caused these features to be misidentified as individual fragmentary systems in the early absorption studies of nitrogen [27–29].

The  $\Delta v$  transitions of an anharmonic oscillator will be linear with slope  $-2 \cdot \Delta v \cdot \omega_e x_e$ , where  $\omega_e x_e$  is the first anharmonic constant [43]. Fitting the least perturbed sections of each positive

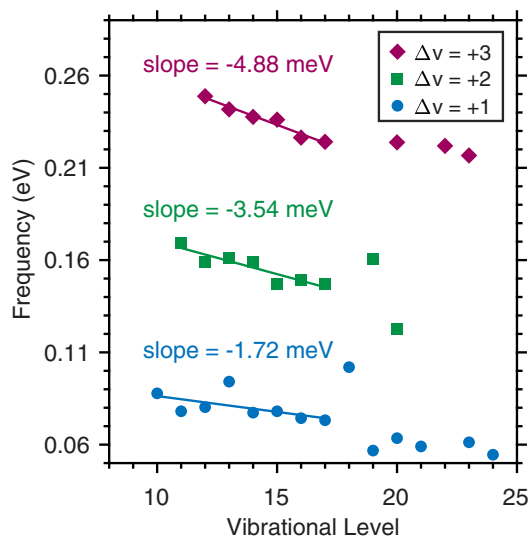


**Fig. 8.** The measured quantum beating frequencies in each  $b'$  vibrational state for the  $\Delta v = +1$  (blue circles),  $+2$  (green squares), and  $+3$  (maroon diamonds) transitions. The unperturbed portions of the coupling frequencies below  $v = 17$  are fit to lines. The measured slopes correspond to  $-2 \cdot \Delta v \cdot \omega_e x_e$ , giving an average  $\omega_e x_e$  value of  $0.85 (\pm 0.03)$  meV to describe the anharmonicity of the  $b'$  potential energy curve in this energy range (see text). (For interpretation of the references to color in this figure legend, the reader is referred to the web version of this article.)

$\Delta v = 1, 2$  and  $3$  transition (illustrated by the solid lines in Fig. 8) results in  $\omega_e x_e$  values of  $0.855, 0.885,$  and  $0.813$  meV, respectively. The average of these measurements,  $0.85 (\pm 0.03)$  meV, is considerably different from the reported  $\omega_e x_e$  value of  $0.55421$  meV obtained from fitting the entire  $b'$  vibrational manifold from  $v = 0$  to  $28$  [28]. However, it is quite close to the value that would be extracted from the frequencies predicted from the known vibrational positions in the smaller  $v = 10$ – $16$  range, where the average anharmonic constant of these three  $\Delta v$  transitions is  $0.89 (\pm 0.05)$  meV.

Besides the obvious perturbations in the  $b'$  state vibrational spacing that limit this analysis for nitrogen, the curvature that develops for the fundamental transition of the higher  $b'$  vibrational levels in Fig. 8 suggests that higher order anharmonic terms are necessary to completely characterize the vibrational energies levels and dynamics. Critically, while the current experimental measurement of  $\omega_e x_e$  is somewhat limited due to its basis on relatively few vibrational levels, these are exactly the levels that are most strongly excited by the XUV pulse. Therefore, this local anharmonicity is what shapes the motion of the nuclear wavepacket excited in the  $b'$  vibrational well.

## 6. Conclusions

A coherent superposition of bound electronic states in nitrogen was prepared by an attosecond XUV pulse. The dynamics of the resulting wavepacket were probed in an ATA measurement, in which a time delayed NIR pulse modifies the structure of the wavepacket by coupling to neighboring states. Pronounced 50 fs oscillations in the ATA spectra of the bound states of nitrogen are due to nuclear dynamics in the  $b' \ ^1\Sigma_u^+$  valence state. The quantum beats observed in individual vibrational levels of this state allow the direct observation of the anharmonicity of this potential well and provide clear evidence of vibrational levels of mixed valence/Rydberg character. A NIR-induced coupling pathway that leads to the observation of the quantum beats is proposed and tested using a many-curve model. This relatively simple model, based on the Born-Oppenheimer approximation, is found to well reproduce

the bound state dynamics of the nuclear wavepacket far from the ionization potential using only 12 electronic states. A simplified 3-curve model is able to highlight the influence of internuclear distance-dependent coupling in the time dependent absorption measurements of the  $b' \ ^1\Sigma_u^+$  valence state molecular wavepacket. This experiment in a simple diatomic molecule demonstrates the possibility of using attosecond transient absorption as a structural tool to characterize the potential wells of more complicated electronic states of larger molecules through the time-dependent observation of their electronic and nuclear dynamics.

Using ATA as a spectroscopic technique to obtain electronic structure in this manner builds on a long history of the study of bound state vibrational wavepackets in molecules, in which femtosecond pulses in the ultraviolet, visible, and infrared allow access to low-lying excited states [44,45]. Especially in congested or perturbed spectral regions, the successes of time-resolved techniques over high resolution static spectroscopy lie in their abilities to separate rotational and vibrational dynamics due to their differing timescales and observe dynamics in an additional frequency domain [46–48]. ATA spectroscopy can be used to extend this multidimensional treatment into the XUV regime [49], where the high time resolution of the technique allows ultrafast electronic dynamics to be separated from slower nuclear dynamics.

## Acknowledgements

Experimental work was supported by the U.S. Department of Energy, Office of Basic Energy Sciences, Chemical Sciences, Geosciences, and Biosciences Division, through Award # DE-AC02-05CH11231. The numerical results presented in this work were obtained at the Centre for Scientific Computing, Aarhus with funding from ERC-StG (Project No. 277767-TDMET), the VKR Center of Excellence QUSCOPE, and FNU (Project No. 0602-01164b). APF acknowledges funding from NSF-GRFP.

## References

- [1] P. Antoine, A. L'Huillier, M. Lewenstein, *Phys. Rev. Lett.* **77** (1996) 1234–1237.
- [2] F. Krausz, M. Ivanov, *Rev. Mod. Phys.* **81** (2009) 163–234.
- [3] K. Ramasesha, S.R. Leone, D.M. Neumark, *Annu. Rev. Phys. Chem.* **67** (2016) 41–63.
- [4] G. Alber, H. Ritsch, P. Zoller, *Phys. Rev. A* **34** (1986) 1058–1064.
- [5] B.M. Garraway, K.-A. Suominen, *Contemp. Phys.* **43** (2002) 97–114.
- [6] B. Feuerstein, U. Thumm, *Phys. Rev. A* **67** (2003) 63408.
- [7] A.R. Beck, D.M. Neumark, S.R. Leone, *Chem. Phys. Lett.* **624** (2015) 119–130.
- [8] E. Constant, D. Garzella, P. Breger, E. Mével, C. Dorrer, C. Le Blanc, F. Salin, P. Agostini, *Phys. Rev. Lett.* **82** (1999) 1668–1671.
- [9] M. Chini, X. Wang, Y. Cheng, Y. Wu, D. Zhao, D.A. Telnov, S.-I. Chu, *Z. Chang, Sci. Rep.* **3** (2013) 1105.
- [10] M. Chini, X. Wang, Y. Cheng, Z. Chang, *J. Phys. B* **47** (2014) 124009.
- [11] W. Cao, E.R. Warrick, D.M. Neumark, S.R. Leone, *New J. Phys.* **18** (2016) 13041.
- [12] X. Wang, M. Chini, Y. Cheng, Y. Wu, X.-M. Tong, *Z. Chang, Phys. Rev. A* **87** (2013) 63413.
- [13] A.R. Beck, B. Bernhardt, E.R. Warrick, M. Wu, S. Chen, M.B. Gaarde, K.J. Schafer, D.M. Neumark, S.R. Leone, *New J. Phys.* **16** (2014) 113016.
- [14] S. Chen, M.J. Bell, A.R. Beck, H. Mashiko, M. Wu, A.N. Pfeiffer, M.B. Gaarde, D.M. Neumark, S.R. Leone, K.J. Schafer, *Phys. Rev. A* **86** (2012) 63408.
- [15] M. Bell, A. Beck, H. Mashiko, D.M. Neumark, S.R. Leone, *J. Mod. Opt.* **60** (2013) 1506–1516.
- [16] C. Ott, A. Kaldun, L. Argenti, P. Raith, K. Meyer, M. Laux, Y. Zhang, A. Blättermann, S. Hagstötz, T. Ding, R. Heck, J. Madroñero, F. Martín, T. Pfeifer, *Nature* **516** (2014) 374–378.
- [17] H. Wang, M. Chini, S. Chen, C.H. Zhang, F. He, Y. Cheng, Y. Wu, U. Thumm, *Z. Chang, Phys. Rev. Lett.* **105** (2010) 143002.
- [18] B. Bernhardt, A.R. Beck, X. Li, E.R. Warrick, M.J. Bell, D.J. Haxton, C.W. McCurdy, D.M. Neumark, S.R. Leone, *Phys. Rev. A* **89** (2014) 23408.
- [19] X. Li, B. Bernhardt, A.R. Beck, E.R. Warrick, A.N. Pfeiffer, M. Justine Bell, D.J. Haxton, C. William McCurdy, D.M. Neumark, S.R. Leone, *J. Phys. B: At. Mol. Opt. Phys.* **48** (2015) 125601.
- [20] E.R. Warrick, W. Cao, D.M. Neumark, S.R. Leone, *J. Phys. Chem. A* **120** (2016) 3165–3174.
- [21] M. Reduzzi, W. Chu, C. Feng, A. Dubrouil, J. Hummert, F. Calegari, F. Frassetto, L. Poletto, O. Kornilov, M. Nisoli, C.-D. Lin, G. Sansone, *J. Phys. B: At. Mol. Opt. Phys.* **49** (2016) 65102.

- [22] Y. Cheng, M. Chini, X. Wang, A. González-Castrillo, A. Palacios, L. Argenti, F. Martín, Z. Chang, *Phys. Rev. A* 94 (2016) 23403.
- [23] J.E. Bækthøj, L. Yue, L.B. Madsen, *Phys. Rev. A* 91 (2015) 43408.
- [24] J.E. Bækthøj, L.B. Madsen, *Phys. Rev. A* 92 (2015) 23407.
- [25] J.E. Bækthøj, L.B. Madsen, *Phys. Rev. A* 94 (2016) 43414.
- [26] H. Lefebvre-Brion, R. Field, *The Spectra and Dynamics of Diatomic Molecules: Revised and Enlarged Edition*, Elsevier Inc., 2004.
- [27] P.K. Carroll, C.P. Collins, *Can. J. Phys.* 47 (1969) 563–589.
- [28] P.K. Carroll, C.P. Collins, K. Yoshino, *J. Phys. B: At. Mol. Phys.* 3 (1970) L127–L131.
- [29] P.K. Carroll, K. Yoshino, *J. Phys. B: At. Mol. Phys.* 5 (1972) 1614–1633.
- [30] W.F. Chan, G. Cooper, R.N.S. Sodhi, C.E. Brion, *Chem. Phys.* 170 (1993) 81–97.
- [31] H. Mashiko, S. Gilbertson, C. Li, S.D. Khan, M.M. Shakya, E. Moon, Z. Chang, *Phys. Rev. Lett.* 100 (2008) 103906.
- [32] P.J. Linstrom, W.G. Mallard, NIST Stand. Ref. Database Number 69 (2016).
- [33] P. Jørgensen, H.J.A. Jensen, J. Olsen, *J. Chem. Phys.* 89 (1988) 3654.
- [34] H. Hetttema, H.J.A. Jensen, P. Jørgensen, J. Olsen, *J. Chem. Phys.* 97 (1992) 1174.
- [35] R.A. Kendall, T.H. Dunning Jr., R.J. Harrison, *J. Chem. Phys.* 96 (1992) 6796–6806.
- [36] K. Aidas, C. Angeli, K.L. Bak, V. Bakken, R. Bast, L. Boman, O. Christiansen, R. Cimiraglia, S. Coriani, P. Dahle, E.K. Dalskov, U. Ekström, T. Enevoldsen, J.J. Eriksen, P. Ettenhuber, B. Fernández, L. Ferrighi, H. Fliegl, L. Frediani, K. Hald, A. Halkier, C. Hättig, H. Heiberg, T. Helgaker, A.C. Hennum, H. Hetttema, E. Hjertenæs, S. Høst, I.M. Høyvik, M.F. Iozzi, B. Jansik, H.J.A. Jensen, D. Jonsson, P. Jørgensen, J. Kauczor, S. Kirpekar, T. Kjærgaard, W. Klopper, S. Knecht, R. Kobayashi, H. Koch, J. Kongsted, A. Krapp, K. Kristensen, A. Ligabue, O.B. Lutnæs, J.I. Melo, K.V. Mikkelsen, R.H. Myhre, C. Neiss, C.B. Nielsen, P. Norman, J. Olsen, J.M.H. Olsen, A. Osted, M.J. Packer, F. Pawłowski, T.B. Pedersen, P.F. Provasi, S. Reine, Z. Rinkevicius, T.A. Ruden, K. Ruud, V.V. Rybkin, P. Salek, C.C. M. Samson, A.S. de Merás, T. Saue, S.P.A. Sauer, B. Schimmelpfennig, K. Sneskov, A.H. Steindal, K.O. Sylvester-Hvid, P.R. Taylor, A.M. Teale, E.I. Tellgren, D.P. Tew, A.J. Thorvaldsen, L. Thøgersen, O. Vahtras, M.A. Watson, D.J.D. Wilson, M. Ziolkowski, H. Ågren, *Wiley Interdiscip. Rev. Comput. Mol. Sci.* 4 (2014) 269–284.
- [37] M.B. Gaarde, C. Buth, J.L. Tate, K.J. Schafer, *Phys. Rev. A* 83 (2011) 13419.
- [38] A. de Lange, R. Lang, W. van der Zande, W. Ubachs, *J. Chem. Phys.* 116 (2002) 7893.
- [39] J. Bominaar, C. Schoemaeker, N. Dam, J.J. Ter Meulen, G.C. Groenenboom, *Chem. Phys. Lett.* 435 (2007) 242–246.
- [40] E.J. Salumbides, A. Khramov, W. Ubachs, *J. Phys. Chem. A* 113 (2009) 2383–2386.
- [41] K. Dressler, *Can. J. Phys.* 47 (1969) 547–561.
- [42] D. Stahel, M. Leoni, K. Dressler, *J. Chem. Phys.* 79 (1983) 2541–2558.
- [43] G. Herzberg, *Molecular Spectra and Molecular Structure: I Spectra of Diatomic Molecules*, second ed., D. Van Nostrand Company Inc, Princeton, NJ, 1950.
- [44] A.H. Zewail, *J. Phys. Chem. A* 104 (2000) 5660–5694.
- [45] K. Ohmori, *Annu. Rev. Phys. Chem.* 60 (2009) 487–511.
- [46] J.R. Andrews, R.M. Hochstrasser, H.P. Trommsdorff, *Chem. Phys.* 62 (1981) 87–101.
- [47] M. Gruebele, A.H. Zewail, *J. Chem. Phys.* 98 (1993) 883–902.
- [48] P. Hamm, M. Lim, W.F. DeGrado, R.M. Hochstrasser, *J. Chem. Phys.* 112 (2000) 1907–1916.
- [49] W. Cao, E.R. Warrick, A. Fidler, D.M. Neumark, S.R. Leone, *Phys. Rev. A* 94 (2016) 53846.